![GFZ Helmholtz-Zentrum POTSDAM logo]

Originally published as:

Impact of oceanic warming on electromagnetic oceanic tidal signals: A CMIP5 climate model-based sensitivity study

J. Saynisch[1] (ID)**, J. Petereit[1]** (ID)**, C. Irrgang[1,2]** (ID)**, and M. Thomas[1,2]**

[1]GFZ German Research Centre for Geosciences, Potsdam, Germany, [2]Institute of Meteorology, Freie Universität Berlin, Berlin, Germany

Abstract In contrast to ocean circulation signals, ocean tides are already well detectable by electromagnetic measurements. Oceanic electric conductivities from the Coupled Model Intercomparison Project Phase 5 (CMIP5) climate simulations are combined with tidal currents of M2 and O1 to estimate electromagnetic tidal signals and their sensitivity to global warming. Ninety-four years of global warming leads to differences of ± 0.3 nT in tidal magnetic amplitudes and ± 0.1 mV/km in the tidal electric amplitudes at sea level. Locally, the climate-induced changes can be much higher, e.g., $+1$ nT in the North Atlantic. In general, all studied electromagnetic tidal amplitudes show large-scale climate-induced anomalies that are strongest in the Northern Hemisphere and amount to 30% of their actual values. Consequently, changes in oceanic electromagnetic tidal amplitudes should be detectable in electromagnetic records. Electric and magnetic signals, as well as tides of different frequencies, contain complementary regional information.

Plain Language Summary Ocean water is a good conductive medium. Ocean water flow through Earth's ambient magnetic field generates measurable electromagnetic signals. By using state of the art Coupled Model Intercomparison Project Phase 5 climate predictions, climate change-induced variations in seawater electric conductivity are calculated. Since these conductivity variations are slow and hard to separate in electromagnetic observations, the derived electric conductivity is combined with ocean tide velocities. Tides are since long detectable with magnetometer observations. We calculate the respective electromagnetic ocean tidal signals and relate their anomalies to climate change. We conclude that climate impact should be detectable in electromagnetic observations, even from space.

1. Introduction

Saline ocean water is an electrically conductive medium. Movement of ocean waters through Earth's ambient magnetic field generates magnetic fields of several nanotesla (nT) and electric fields of several millivolt per kilometer (mV/km) at sea level. Oceanic electromagnetic (EM) signals are sensitive to seawater's velocity and electric conductivity. Quantification of these sensitivities can be used to infer respective information about the ocean from EM measurements. This is especially important now, since new satellite missions allow a global view of the ocean with unprecedented precision [*Friis-Christensen et al.*, 2006]. Nonetheless, the study of oceanic electromagnetic tidal signals has a long oceanographic history [e.g., *Larsen*, 1968; *Sanford*, 1971, and references therein]. Among the oceanographic features, the M2 tide induces the strongest EM signal (± 6 nT at sea level) [e.g., *Maus and Kuvshinov*, 2004]. Due to their periodicity, tides are well identifiable in magnetometer measurements and detectable even from space [*Tyler et al.*, 2003; *Sabaka et al.*, 2016]. EM signals from the general ocean circulation are of comparable strength (± 5 nT at sea level) [e.g., *Irrgang et al.*, 2016] but contain a large static component which is hard to separate from other static or slowly changing EM sources like crustal magnetization [*Hemant and Maus*, 2005] or Earth's background magnetic field [*Gillet et al.*, 2010]. The separable, i.e., temporally variable, component is much smaller (± 0.5 nT at sea level) [e.g., *Manoj et al.*, 2006]. Furthermore, ocean circulation signals are more irregular than tidal signals, which further hinders their detection, particularly from space.

Despite the mentioned difficulties, oceanic EM signals can be very useful in monitoring the ocean. Many studies have inferred oceanic transports from in situ measurements, such as seafloor voltage cables [e.g., *Larsen*, 1991; *Fujii et al.*, 1995]. With the launch of the new satellite mission Swarm [*Friis-Christensen et al.*, 2006; *Olsen et al.*, 2007], and with the deployment of new terrestrial EM stations, smaller oceanographic features are

extractable for current research. For example, tides weaker than M2 are now observable from space [*Sabaka et al.*, 2016]; tsunamis are detectable in coastal and seafloor EM measurements [*Manoj et al.*, 2010; *Schnepf et al.*, 2016], and electromagnetic oceanic tidal signals (EMOTS) are used to constrain the conductivity of the lithosphere and upper mantle [*Schnepf et al.*, 2015; *Grayver et al.*, 2016].

The sensitivity of EMOTS to seawater temperature and salinity renders them a useful tool to monitor ocean climate. *Saynisch et al.* [2016] demonstrated a method that uses the easily detectable EMOTS to reveal slowly varying oceanographic features. Their study simulated and analyzed effects of Greenland glacial melting on EMOTS with a very simple freshwater hosing experiment. The authors show in principle that glacial melting has a measurable impact on EMOTS. Other climate change-related effects, such as ocean warming itself and ocean-atmosphere feedbacks, are neglected in their simulations. These effects are considered in this manuscript. Our study uses fully coupled state-of-the-art Earth System Models (ESM) to characterize the impact of global warming on EMOTS. The study is predominantly a sensitivity study. Nonetheless, we comment on the observability of the results.

The incorporated EM models, the climate model, and all additional data needed to generate EMOTS are described in section 2. The ensuing results are presented and discussed in section 3. We close with conclusions and a short summary.

2. Models and Data

Saynisch et al. [2016] show that oceanic tidal velocities (amplitudes, frequencies, and phases) change very little during decades and centuries even under severe climate change. Consequently, the climate impact on EMOTS is mainly attributed to changes in seawater conductivity. Justified by these results, we do not simulate individual tidal velocities for an entire scenario of climate change but use one set of contemporary observation-based tidal velocities for all calculations. Barotropic tidal velocity amplitudes and phases from *Egbert and Erofeeva* [2002] (TPXO8-atlas) are used for this purpose. From the TPXO catalog we use the tide with the strongest electromagnetic signal, the semidiurnal M2 [e.g., *Sabaka et al.*, 2016]. In addition, a diurnal tide was chosen, O1. The O1 induces weaker EMOTS than M2 but diurnal and semidiurnal ocean tides differ in their global resonance pattern and can be used to investigate different oceanic regions.

Note that while K1 generates similar but larger EM signals than O1, the K1 signal is presently harder to separate in magnetic measurements than the O1 mode [*Maus and Kuvshinov*, 2004]. The M2 and O1 velocity fields are bilinearly interpolated onto a regular 1° × 1° grid.

Climate change-induced time variable distributions of ocean conductivity are derived from selected climate simulations of the Coupled Model Intercomparison Project Phase 5 (CMIP5) [*Taylor et al.*, 2012]. The climate projections referred to as Representative Concentration Pathways (RCPs) used in this study cover the years from 2006 to 2100 and describe a scenario of high greenhouse gas emission without mitigation (RCP 8.5, i.e., business as usual) [*Riahi et al.*, 2011].

In general, the CMIP5 scenarios are calculated by ensembles of different model codes and model configurations. We follow this approach and repeat our calculations for selected members of the CMIP5 model range. Namely, we use output from HadGEM2-ES [*Collins et al.*, 2008] from Met Office Hadley Centre and Instituto Nacional de Pesquisas Espaciais; we use HadGEM2-AO [*Collins et al.*, 2008] from the National Institute of Meteorological Research and Korea Meteorological Administration; and we use GFDL-ESM2 M [*Dunne et al.*, 2012, 2013] from NOAA Geophysical Fluid Dynamics Laboratory. This small selection of models is used as a check of the robustness of our findings. It will become evident if the different models, differing in their numerical formulation and complexity, give very different results. HadGEM2-AO couples modules for the troposphere, land surface, hydrology, aerosols, ocean, and sea ice. HadGEM2-ES is an ESM. It additionally includes modules for the terrestrial carbon cycle, ocean biogeochemistry, and atmospheric chemistry. GFDL-ESM2 M has similar components as HadGEM2-ES, but it also has an advanced ocean model component that simulates the oceanic carbon cycle.

None of the CMIP5 models include a dynamic, interactive land-ice module. As a result, the freshwater flux due to glacial melting is greatly underestimated [*Little et al.*, 2016]. As far as the ocean's forcing is concerned, all of the used climate simulations generate changes in evaporation, precipitation, river runoff, atmospheric heat flux, and wind stress. These changes are dynamically coupled to the ocean and influence the ocean's global

circulation, heat content, sea ice, and sea level. As a consequence of all these effects, the ocean's salinity (S) and temperature (T) distributions are characteristically altered.

Monthly S and T fields of the CMIP5-RCP 8.5 simulations are annually averaged and interpolated bilinearly onto a regular 1°×1° grid. Electric seawater conductivity is calculated from T, S, and hydrostatic pressure using the R-package `oce` [*Kelley and Richards*, 2015], which incorporates the Gibbs-SeaWater equation (TEOS-10) [*IOC et al.*, 2010]. The modeling of the EM induction process is identical to the procedure described in *Saynisch et al.* [2016]. Therefore, only a summary is given here. The CMIP5-based electric seawater conductivity is multiplied with Earth's ambient magnetic field, as well as with the tidal velocity amplitudes and phases from TPXO8-atlas. The product is integrated vertically to derive electric tidal currents. For this step, estimates of Earth's ambient magnetic field from International Geomagnetic Reference Field 12th edition [*Thébault et al.*, 2015] up to degree and order 13 are used. Note that secular variations of Earth's ambient magnetic field will also result in slowly varying EMOTS anomalies. Earth's ambient magnetic field contributes only to the generation of the oceanic electric currents, i.e., the sources of the EM induction process [e.g., *Chave and Luther*, 1990]. This contribution is linear and well known for real observation times [e.g., *Gillet et al.*, 2010]. This paper omits the superposing effect of secular variation to study climate-induced EMOTS deviations only. Consequently, in this paper, Earth's ambient magnetic field is the same for all calculations of electric tidal currents. However, secular variation should be filtered from real tidal EM observations before searching for respective climate change-induced trends.

The resultant 1°×1° tidal electric currents are used to force the 3-D induction model of *Kuvshinov* [2008]. A thin ocean and sediment layer of spatially variable electric conductance is assumed [*Laske and Masters*, 1997; *Everett et al.*, 2003] in addition to a 1-D spherically symmetric mantle conductivity [*Püthe et al.*, 2015]. In the induction model, EM fields are calculated in frequency space by a volume integral equation approach. We calculate 1°×1° EM fields at sea level and at satellite altitude (430 km above sea level).

3. Results and Discussion

Oceanic tidal patterns are the result of a resonance between forcing period on the one hand and local Kelvin wave speed in combination with ocean basin geometry on the other hand. To study different tidal patterns, semidiurnal and diurnal tides are analyzed in this study. From each of the two tidal families we choose one representative tide, i.e., M2 and O1. Note that tidal signals from the semidiurnal family are already detected in satellite magnetometer observations [*Tyler et al.*, 2003; *Sabaka et al.*, 2016]. The EMOTS of M2 and O1 are calculated as described in section 2 (see supporting information, Figures S1 and S2). Pattern and amplitudes of the EMOTS are within the range of reported values [e.g., *Maus and Kuvshinov*, 2004; *Sabaka et al.*, 2015]. The radial M2 (O1) magnetic component shows the typical values and pattern around ±5 nT (±2 nT) at sea level. The magnetic x and y components are weaker and show values around ±3 nT (±1 nT) at sea level. The oceanic tidal electric fields show values around 1 mV/km (0.5 mV/km) for all components. Near the coasts, the electric field anomalies can be much higher due to the high land-ocean conductivity contrast. As with the magnetic fields, the electric field's values and pattern correspond to the literature [e.g., *Kuvshinov et al.*, 2006]. In general, the EMOTS are not globally uniform. While the electric fields peak at the coasts, the magnetic signals tend to peak in the open ocean. In addition, magnetic fields have the advantage of being measurable at satellite altitude (supporting information, Figures S9–S11).

Due to the different resonance tidal wave and ocean basin, the M2-EMOTS and O1-EMOTS differ in their geographical distribution. For example, the M2 pattern is strong in the northern Atlantic and around Australia. The O1 pattern is strong in higher latitudes such as the Southern Ocean and the Arctic and in the Kuroshio region. After the calculation of EMOTS throughout the RCP 8.5 climate scenario, the EMOTS from year 2006 are subtracted from the respective year 2100 values.

The resulting, i.e., climate change-induced, differences are plotted in Figure 1 (top row) for the radial component of the induced magnetic field at sea level. The x and y magnetic components show slightly lesser climate impact but similar patterns (supporting information, Figure S3). The magnetic field M2 (O1) differences amount to ±0.3 nT (±0.1 nT) in large-scale averages. Locally, the climate-induced M2 EMOTS changes can reach +1.0 nT, e.g., in the Labrador Sea and around Spitsbergen. The respective O1 EMOTS changes reach 0.5 nT, e.g., in the Ross Sea. These signals are well above contemporary measurement precisions (e.g., 0.1 nT) [*Friis-Christensen et al.*, 2006; *Olsen et al.*, 2007]. Naturally, the values become smaller when propagated to satellite altitude. However, at Swarm altitude the M2 values are still above the estimated precision (supporting
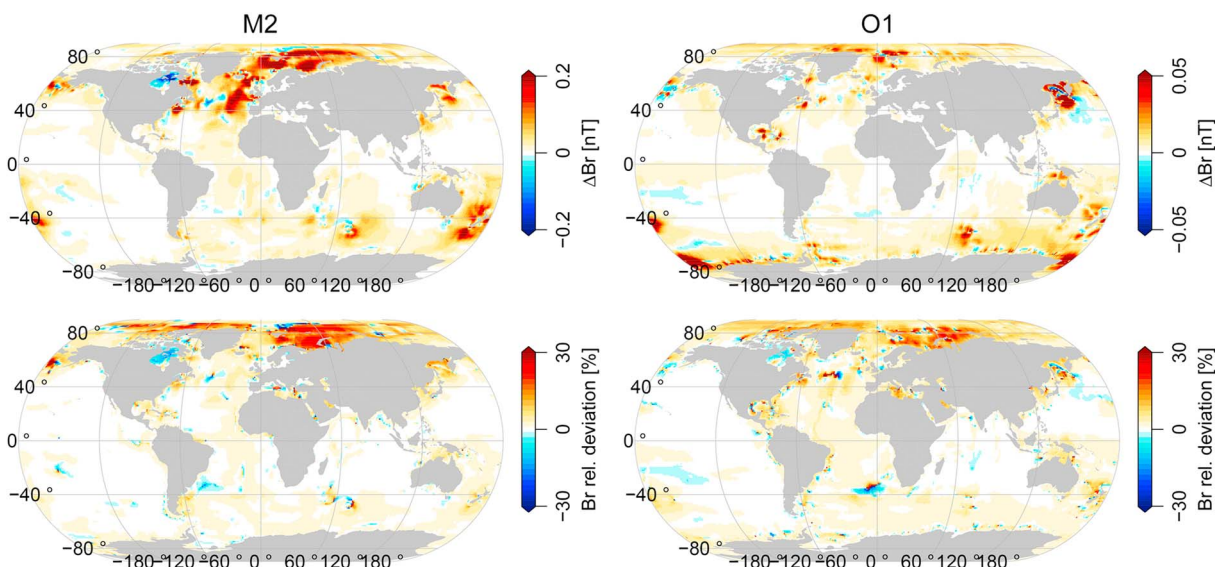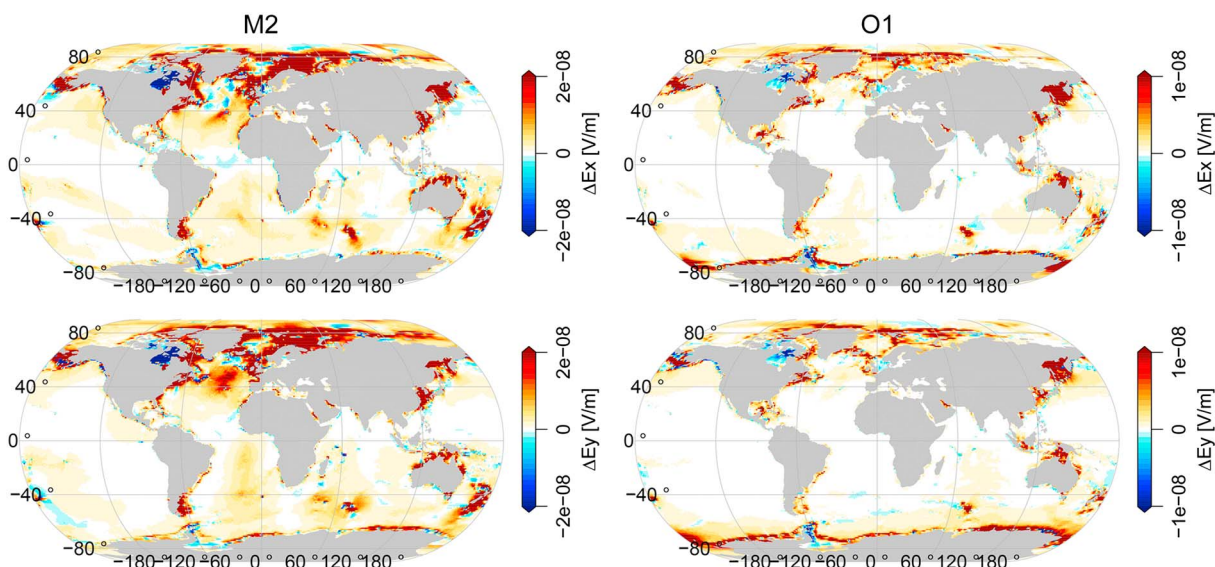
Figure 1. Influence of enhanced greenhouse gas forcing (CMIP5, RCP 8.5) on tidal radial magnetic signals at sea level. (top row) Tidal amplitude differences from HadGEM2-ES (year 2100 minus year 2006). (bottom row) Percentual relative deviation (year 2100 minus year 2006 divided by year 2006). (left column) M2. (right column) O1.

information, Figure S10). The relative deviations of the magnetic anomalies are plotted in Figure 1 (bottom row). The larger relative differences are located in the Northern Hemisphere and amount to +30%.

In contrast to the climate impact on the magnetic field (and in accordance to Maxwell's equations), changes in the tidal electric field are most pronounced in the x and y components (see Figure 2). Here deviations of ±0.1 mV/km can be reported. As with the magnetic field components, the biggest climate impacts are located in the Northern Hemisphere. Nonetheless, high EMOTS anomalies are visible at the coast of Antarctica. Here especially O1 shows an electric field anomaly that is much less pronounced in M2's electric field and that does not exist in the magnetic components. Relative to the EMOTS itself, the climate-induced electric field deviations reach 30% (supporting information, Figure S6).

The global warming-induced EMOTS deviations are robust over the range of tested CMIP5 models (see section 2). These models differ in complexity and resolved Earth systems. However, the models show very

Figure 2. Influence of enhanced greenhouse gas forcing (CMIP5, RCP 8.5) on tidal horizontal electric signals at sea level. Tidal amplitude differences from HadGEM2-ES (year 2100 minus year 2006). (left column) M2. (right column) O1. (top row) E_x. (bottom row) E_y.
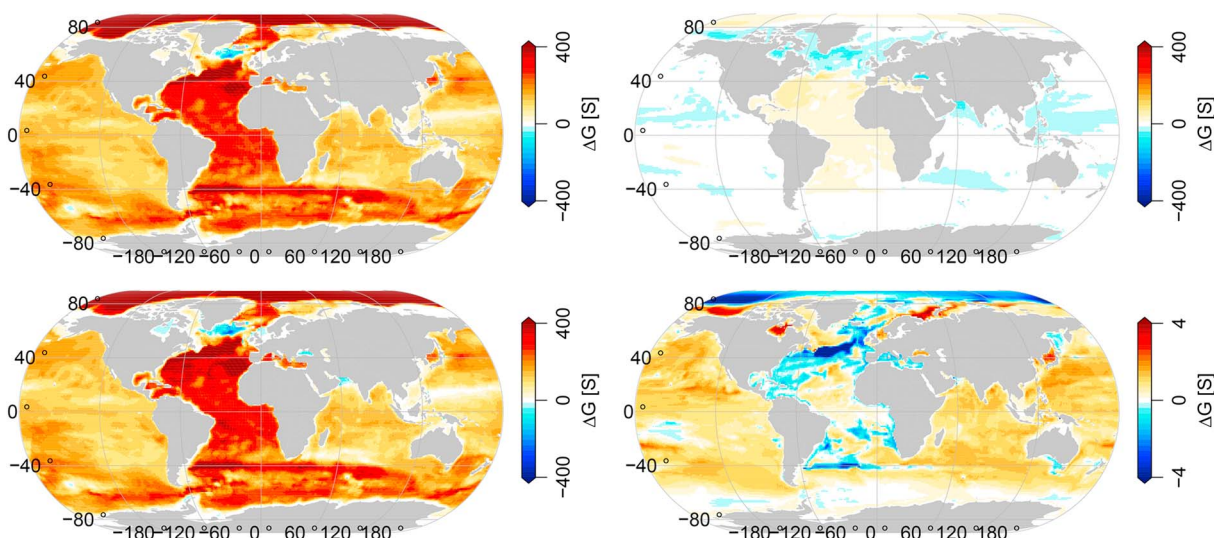
Figure 3. Contribution of 94 years of *T* and *S* changes from CMIP5-RCP 8.5 to changes in oceanic conductance (*G*). (top row) Conductance change due to temperature change only (left). Conductance change due to salinity change only (right). (bottom row) Conductance change due to the combined effect of *T* and *S* change (left). Conductance difference between the combined effect of *T* and *S* change and the sum of the separated *T* and *S* effects (right; note that the plotted range is only 1% of the other plots).

similar climate sensitivities, i.e., patterns and signs, in all six EM components. Nonetheless, the maxima of the climate change impact on EMOTS can deviate among the models by up to 50% (supporting information, Figures S7 and S8).

The values and relative deviations of the magnetic M2 anomalies are comparable in strength to the findings of *Saynisch et al.* [2016, Figures 3 and 4]. However, the location and sign of the M2 magnetic deviation pattern are different to our findings. Both studies show substantial impact in the waters around New Zealand (near the southern geomagnetic pole), north of Europe (near the northern geomagnetic pole), and in the Kuroshio region. Of these regions, only the anomalies north of Japan have the same sign in the two studies. Both studies agree locally in the Agulhas region, Drake Passage, and in parts of the Arctic Ocean. However, the global differences dominate.

The Greenland melting of the *Saynisch et al.* [2016] study leads to cooling and freshening of oceanic waters and consequently resulted in weaker EMOTS in most parts of the globe. The global warming of our study results in stronger EMOTS in most parts of the globe.

Figure 3 analyzes the contribution of *T* and *S* changes to the oceanic conductance *G* of year 2100. Figure 3 (bottom left) shows the conductance difference between 2100 and 2006, i.e., $\Delta G = G(S_2, T_2) - G(S_1, T_1)$. Overall, the conductance is higher in year 2100 than in year 2006. The differences reach up to 400 S. Figure 3 (top row) shows the change in conductance if either *S* or *T* did not deviate from their 2006 values, i.e., $G(S_1, T_2) - G(S_1, T_1)$, respectively, $G(S_2, T_1) - G(S_1, T_1)$. Changes in *S* alone result in small positive and negative conductance changes of a few *S*. The CMIP5 simulations produce seawater freshening (i.e., lower conductivity) only in the upper $\approx$150 m of the ocean, especially in the Arctic and the North Atlantic (not shown).

Changes in *T* alone result in conductance anomalies of up to 400 S, and the distribution is very similar to that of the year 2100's total conductance anomalies (compare the two plots on the left side). The sensitivity of electrical conductance toward *T*, respectively, *S* changes is not linear. To justify the split of conductance anomalies into *T* and *S* contributions, the respective nonlinearity is estimated. Figure 3 (bottom right) shows the difference between the combined effect of *T* and *S* change on the conductance and the superposition of the separated *T* and *S* change effects on conductance (i.e., Figure 3 (top row) is added together, and Figure 3 (bottom left) is subtracted). Errors in the assumption of linearity are most pronounced in the North Atlantic and the Arctic. However, the errors remain below 10 S. Consequently, we conclude that the change in *T*, i.e., the oceanic warming, dominates nearly all of the identified EMOTS anomalies.

However, the ocean circulation under the combined effect of glacial melting [*Saynisch et al.*, 2016] and oceanic warming (this paper) will most likely not be a simple superposition of the circulations that result from the

separated effects. Consequently, the resulting *T* and *S* distributions and the EMOTS anomalies will not be a simple superposition either. The CMIP5 successor CMIP6 aims to couple dynamic and interactive land-ice sheet models into the climate simulations [*Nowicki et al.*, 2016; *Eyring et al.*, 2016]. Until then, we can only conclude that ocean warming (temperature influence on conductivity) and glacial melting (salinity influence on conductivity) show opposing sensitivities and lead to stronger/weaker EMOTS. Both mechanisms have the potential to generate measurable deviations in EMOTS. The combined effect of glacial melting and global warming on EMOTS remains to be evaluated.

4. Summary and Conclusion

Ocean temperatures and salinities from state-of-the-art CMIP5 climate predictions are used to calculate centennial variations in seawater electric conductivity. Since the resultant conductivity variations are slow and hard to separate in electromagnetic observations, the derived electric conductivity is combined with ocean tidal velocities of M2 and O1 to study changes in their electromagnetic amplitudes. Tides are easily separable in magnetometer observations [e.g., *Sabaka et al.*, 2016] or seafloor voltage cables [e.g., *Thomson et al.*, 1986]. We calculate respective electromagnetic ocean tidal signals (EMOTS) and relate their anomalies to the modeled climate change. Ninety-four years of enhanced greenhouse gas forcing results in radial magnetic component differences of ±0.3 nT for M2-EMOTS and ±0.1 nT for O1-EMOTS for large areas at sea level. Locally, the climate-induced M2 EMOTS changes can reach +1.0 nT, e.g., in the Labrador Sea and around Spitsbergen. The respective O1 EMOTS changes reach 0.5 nT, e.g., in the Ross Sea. For shorter time windows, the differences will be smaller, e.g., 0.1 nT per decade. Electric tidal *x, y* components deviate generally by ±0.1 mV/km at sea level. All studied electromagnetic tidal amplitudes show relative differences that are largest in the Northern Hemisphere and amount to 30% and stronger. The anomalies are strong enough to be measured by terrestrial electrometers/magnetometers or spaceborne magnetometers. By comparing different CMIP5 simulations of the same climate scenario, the strongest anomalies show an uncertainty of 10–50%. The overall strengthening of the signals is attributed to the warming of the ocean water and the resultant higher seawater conductivity. The individual O1 and M2 electromagnetic patterns can be used together to monitor warming in different oceanic regions. Due to the large contrast in land conductance and sea conductance, electric tidal amplitudes are much more sensitive to changes in coastal regions than the respective magnetic fields. Consequently, climate change signals may be better observed by coastal seafloor voltage cables [*Baringer and Larsen*, 2001]. In combination with seafloor voltage cables [*Thomson et al.*, 1986] or magnetometer stations [*Maus and Kuvshinov*, 2004; *Schnepf et al.*, 2014] and the magnetic tidal fields that are observable from space [e.g., *Sabaka et al.*, 2016] the presented results could be used to monitor ocean climate change.

Ocean warming and glacial melting have opposing sensitivities and lead to stronger/weaker EMOTS. Which effect truly dominates current and future EMOTS anomalies remains to be evaluated. Until climate models are available that realistically simulate both effects, we can only conclude that glacial melting and oceanic warming both have the potential to generate measurable deviations in EMOTS. In general, long-run electromagnetic measurements should be checked for EMOTS anomalies. If detected, observed EMOTS changes (subject to heat and salinity) could be combined with other integral measurements like altimetry (heat, salinity, and mass) and gravimetry (mass) to assess climate-induced changes in the ocean.

References

Baringer, M. O., and J. C. Larsen (2001), Sixteen years of Florida Current transport at 27°N, *Geophys. Res. Lett.*, *28*(16), 3179–3182.

Chave, A. D., and D. S. Luther (1990), Low-frequency, motionally induced electromagnetic-fields in the ocean 1. Theory, *J. Geophys. Res.*, *95*(C5), 7185–7200.

Collins, W., et al., (2008), Evaluation of the HadGEM2 model, *Tech. Rep. HCTN 74*, Met Office Hadley Centre, Exeter, U. K.

Dunne, J. P., et al. (2012), GFDL's ESM2 global coupled climate-carbon Earth system models. Part I: Physical formulation and baseline simulation characteristics, *J. Clim.*, *25*(19), 6646–6665.

Dunne, J. P., et al. (2013), GFDL's ESM2 global coupled climate-carbon Earth system models. Part II: Carbon system formulation and baseline simulation characteristics, *J. Clim.*, *26*(7), 2247–2267.

Egbert, G. D., and S. Y. Erofeeva (2002), Efficient inverse modeling of barotropic ocean tides, *J. Atmos. Oceanic Technol.*, *19*, 183–204.

Everett, M. E., S. Constable, and C. G. Constable (2003), Effects of near-surface conductance on global satellite induction responses, *Geophys. J. Int.*, *153*(1), 277–286.

Eyring, V., S. Bony, G. A. Meehl, C. A. Senior, B. Stevens, R. J. Stouffer, and K. E. Taylor (2016), Overview of the Coupled Model Intercomparison Project Phase 6 (CMIP6) experimental design and organization, *Geosci. Model Dev.*, *9*, 1937–1958.

Friis-Christensen, E., H. Lühr, and G. Hulot (2006), Swarm: A constellation to study the Earth's magnetic field, *Earth Planets Space*, *58*(4), 351–358.

Fujii, I., L. J. Lanzerotti, H. Utada, H. Kinoshita, J. Kasahara, L. V. Medford, and C. G. Maclennan (1995), Geoelectric power spectra over oceanic distances, *Geophys. Res. Lett.*, *22*(4), 421–424.

Gillet, N., V. Lesur, and N. Olsen (2010), Geomagnetic core field secular variation models, *Space Sci. Rev.*, *155*(1), 129–145.

Grayver, A. V., N. R. Schnepf, A. V. Kuvshinov, T. J. Sabaka, C. Manoj, and N. Olsen (2016), Satellite tidal magnetic signals constrain oceanic lithosphere-asthenosphere boundary, *Sci. Adv.*, *2*(9), e1600798, doi:10.1126/sciadv.1600798.

Hemant, K., and S. Maus (2005), Why no anomaly is visible over most of the continent-ocean boundary in the global crustal magnetic field, *Phys. Earth Planet. Inter.*, *149*(3–4), 321–333.

IOC, SCOR, and APSO (2010), *The International Thermodynamic Equation of Seawater-2010: Calculation and Use of Thermodynamic Properties*, 196 pp., Intergovernmental Oceanographic Commission, Manuals and Guides No. 56, UNESCO, Paris.

Irrgang, C., J. Saynisch, and M. Thomas (2016), Impact of variable seawater conductivity on motional induction simulated with an ocean general circulation model, *Ocean Sci.*, *12*(1), 129–136.

Kelley, D., and C. Richards (2015), *Oce: Analysis of Oceanographic Data*, R package version 0.9-17, CRAN. [Available at https://CRAN.R-project.org/package=oce.]

Kuvshinov, A., A. Junge, and H. Utada (2006), 3-D modelling the electric field due to ocean tidal flow and comparison with observations, *Geophys. Res. Lett.*, *33*, L06314, doi:10.1029/2005GL025043.

Kuvshinov, A. V. (2008), 3-D global induction in the oceans and solid Earth: Recent progress in modeling magnetic and electric fields from sources of magnetospheric, ionospheric and oceanic origin, *Surv. Geophys.*, *29*(2), 139–186.

Larsen, J. C. (1968), Electric and magnetic fields induced by deep sea tides, *Geophys. J. R. Astron. Soc.*, *16*, 47–10.

Larsen, J. C. (1991), Transport measurements from in-service undersea telephone cables, *IEEE J. Ocean. Eng.*, *16*(4), 313–318.

Laske, G., and G. Masters (1997), A global digital map of sediment thickness, *Eos Trans. AGU*, *78*(46), F483.

Little, C. M., C. G. Piecuch, and A. H. Chaudhuri (2016), Quantifying greenland freshwater flux underestimates in climate models, *Geophys. Res. Lett.*, *43*, 5370–5377, doi:10.1002/2016GL068878.

Manoj, C., A. Kuvshinov, S. Maus, and H. Lühr (2006), Ocean circulation generated magnetic signals, *Earth Planets Space*, *58*(4), 429–437.

Manoj, C., A. Kuvshinov, S. Neetu, and T. Harinarayana (2010), Can undersea voltage measurements detect tsunamis?, *Earth Planets Space*, *62*(3), 353–358.

Maus, S., and A. Kuvshinov (2004), Ocean tidal signals in observatory and satellite magnetic measurements, *Geophys. Res. Lett.*, *31*, L15313, doi:10.1029/2004GL020090.

Nowicki, S. M. J., A. Payne, E. Larour, H. Seroussi, H. Goelzer, W. Lipscomb, J. Gregory, A. Abe-Ouchi, and A. Shepherd (2016), Ice Sheet Model Intercomparison Project (ISMIP6) contribution to CMIP6, *Geosci. Model Dev.*, *9*(12), 4521–4545.

Olsen, N., T. J. Sabaka, and L. R. Gaya-Pique, (2007), Study of an improved comprehensive magnetic field inversion analysis for Swarm — Final report, *Tech. Rep.*, Danisch National Science Center, Lungby, Denmark.

Püthe, C., A. Kuvshinov, A. Khan, and N. Olsen (2015), A new model of Earth's radial conductivity structure derived from over 10 yr of satellite and observatory magnetic data, *Geophys. J. Int.*, *203*(3), 1864–1872.

Riahi, K., S. Rao, V. Krey, C. Cho, V. Chirkov, G. Fischer, G. Kindermann, N. Nakicenovic, and P. Rafaj (2011), RCP 8.5—A scenario of comparatively high greenhouse gas emissions, *Clim. Change*, *109*(1), 33.

Sabaka, T. J., R. H. Tyler, and N. Olsen (2016), Extracting ocean-generated tidal magnetic signals from swarm data through satellite gradiometry, *Geophys. Res. Lett.*, *43*, 3237–3245, doi:10.1002/2016GL068180.

Sabaka, T. J., N. Olsen, R. H. Tyler, and A. Kuvshinov (2015), CM5, a pre-Swarm comprehensive geomagnetic field model derived from over 12 yr of CHAMP, Orsted, SAC-C and observatory data, *Geophys. J. Int.*, *200*(3), 1596–1626.

Sanford, T. B. (1971), Motionally induced electric and magnetic fields in the sea, *J. Geophys. Res.*, *76*(15), 3476–3492.

Saynisch, J., J. Petereit, C. Irrgang, A. Kuvshinov, and M. Thomas (2016), Impact of climate variability on the tidal oceanic magnetic signal—A model based sensitivity study, *J. Geophys. Res. Oceans*, *121*, 5931–5941, doi:10.1002/2016JC012027.

Schnepf, N. R., C. Manoj, C. An, H. Sugioka, and H. Toh (2016), Time-frequency characteristics of tsunami magnetic signals from four Pacific Ocean events, *Pure and Appl. Geophys.*, *173*(12), 3935–3953.

Schnepf, N. R., C. Manoj, A. Kuvshinov, H. Toh, and S. Maus (2014), Tidal signals in ocean-bottom magnetic measurements of the Northwestern Pacific: Observation versus prediction, *Geophys. J. Int.*, *198*(2), 1096–1110.

Schnepf, N. R., A. Kuvshinov, and T. Sabaka (2015), Can we probe the conductivity of the lithosphere and upper mantle using satellite tidal magnetic signals?, *Geophys. Res. Lett.*, *42*, 3233–3239, doi:10.1002/2015GL063540.

Taylor, K. E., R. J. Stouffer, and G. A. Meehl (2012), An overview of CMIP5 and the experiment design, *Bull. Am. Meteorol. Soc.*, *93*, 485–498.

Thébault, E., et al. (2015), International geomagnetic reference field: The 12th generation, *Earth Planets Space*, *67*(1), 79.

Thomson, D. J., L. J. L. J. Lanzerotti, C. G. M. A. Medford, L. V. Maclennan, and G. P. Gregori (1986), Study of tidal periodicities using a transatlantic telecommunications cable, *Geophys. Res. Lett.*, *13*, 525–528.

Tyler, R. H., S. Maus, and H. Luhr (2003), Satellite observations of magnetic fields due to ocean tidal flow, *Science*, *299*(5604), 239–241.